Supplementary Information for

Reduction of precious metal ions in aqueous solutions by contact-electro-catalysis

Yusen Su,[1,2,10], Andy Berbille[1,2,10], Xiao-Fen Li[3,1,10], Jinyang Zhang[1,2,10], MohammadJavad PourhosseiniAsl[1,4], Huifan Li[1,5], Zhanqi Liu[1,6], Shunning Li[7], Jianbo Liu[3], Laipan Zhu[1,2,*], Zhong Lin Wang[1,2,8,9,*]

[1] CAS Center for Excellence in Nanoscience, Beijing Institute of Nanoenergy and Nanosystems, Chinese Academy of Sciences, Beijing 101400, China

[2] School of Nanoscience and Technology, University of Chinese Academy of Sciences, Beijing 100049, China

[3] China Key Laboratory of Advanced Materials (MOE), School of Materials Science and Engineering, Tsinghua University, Beijing, 100084, China

[4]Department of Materials Science and Engineering, College of Engineering, Peking University, 100871, Beijing, China

[5] Center on Nanoenergy Research, School of Physical Science and Technology, Guangxi University, Nanning 530004, China

[6] School of Physical Science and Technology, Lanzhou University, Lanzhou 730000, China

[7] School of Advanced Materials, Shenzhen Graduate School, Peking University, Shenzhen, 518055, China

[8] Yonsei Frontier Lab, Yonsei University, Seoul 03722, Republic of Korea

[9]School of Materials Science and Engineering, Georgia Institute of Technology, Atlanta, GA 30332-0245, USA

[10] These authors contributed equally.

**Corresponding authors. Email: zhong.wang@mse.gatech.edu (Z.L.W.); zhulaipan@binn.cas.cn (L.Z.)

The PDF file includes:

Supplementary Note 1: Details of Contact-electro-catalysis

The principle of contact-electro-catalysis is based on the exchange electrons occurring when water contacts the surface of a dielectric insulator[1]. When a water molecule contacts a polymer the electron clouds of the solid and the liquid could overlap[2]. At this point, if the electron affinity of the polymer is sufficiently high, then 1 electron can be transferred from the molecule of water to the polymer chain (**Equation 1**). Thereafter the water radical cation thus formed can react with a water molecule and for a hydronium cation and a hydroxyl radical (**Equation 2**), and the polymer is now charged (symbolized by an asterisk in **Equation 1**)[3].

(1) $H_2O_{(l)} + FEP_{(s)} \xrightarrow{SL-CE} H_2O^{\bullet+}_{(aq)} + FEP^{*}_{(s)}$

(2) $H_2O^{\bullet+}_{(aq)} + H_2O_{(l)} \rightarrow H_3O^{+}_{(aq)} + HO^{\bullet}_{(aq)}$

Under ultrasonic conditions[4], or if the material is exposed to visible light[5], there is a probability that the electron gets excited from the surface of the charge polymer towards the bulk of water (**Equation 3**)[3]. This electron can then react with O_2 gas dissolved in the solution to form superoxide radicals (**Equation 4**)[3].

(3) $FEP^{*}_{(s)} \xrightarrow{\substack{photons,\\ phonons,\\ heat}} e^- + FEP_{(s)}$

(4) $O_{2_{(g)}} + e^- \rightarrow O^{\bullet-}_{2_{(aq)}}$

Under ultrasonic conditions, the contact-separation cycle that allows for the exchange of electrons by contact-electrification between water and the dielectric insulator (catalyst) is provided by the high frequency generation of microbubbles in the vicinity of or at the surface of the catalyst[6]. When the bubble grows at/near the surface of the solid, it chasses the water while the electrons are ejected from the surface upon absorption of phonon, heat or light[3]. When the bubble collapses, not only does the water contacts the solid again, which allows for 1 more cycle of electron transfers, but it may do it with a high force or velocity owing to the formation of a high pressure microjet[3]. As long as the material and aqueous solutions are exposed to ultrasonication, the catalytic cycle continues. In this case, a high number of electrons are generated, as illustrated by the EPR data reported in **Fig. 1d** in the main text. In this case, it is possible to reduce the metals metal ions mentioned in the main text (**Equation 5**).

(5) $M^{n+}_{(aq)} + ne^- \rightarrow M^{0}_{(s)}$

It is worth noting other mechanisms may contribute to effects of CEC, including the contribution of the

corona of bubbles on solid surface[7], or exchange of hydroxyl functional groups between water and the surface of SiO_2[8].

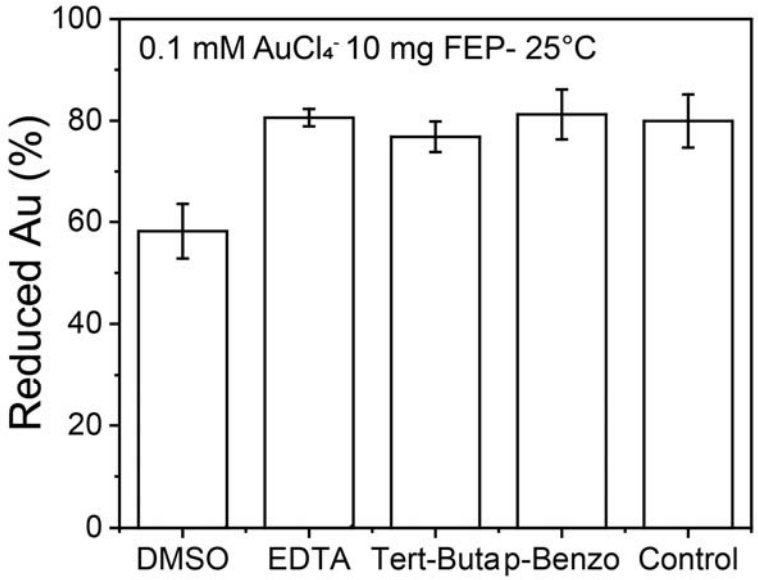

Supplementary Fig. 1 | Evolution of Au concentration in conditions of various radical scavengers. Ter-butanol, p-benzoquinone, DMSO, and EDTA-2Na, are regarded as superoxide radical, hydroxide radical, electron, and proton scavengers, respectively. For all figures, error bars represent standard deviations for 3 reproduced experiments.

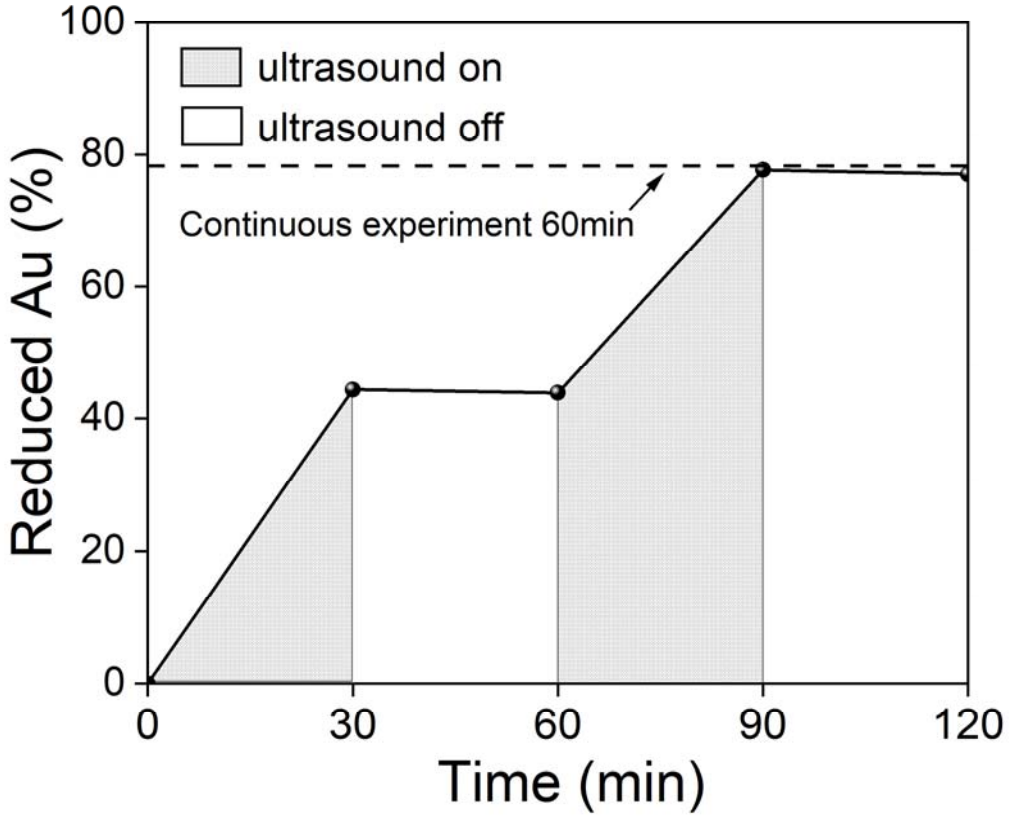

Supplementary Fig. 2 | Intermittent and continuous reaction in 120 W ultrasonication.

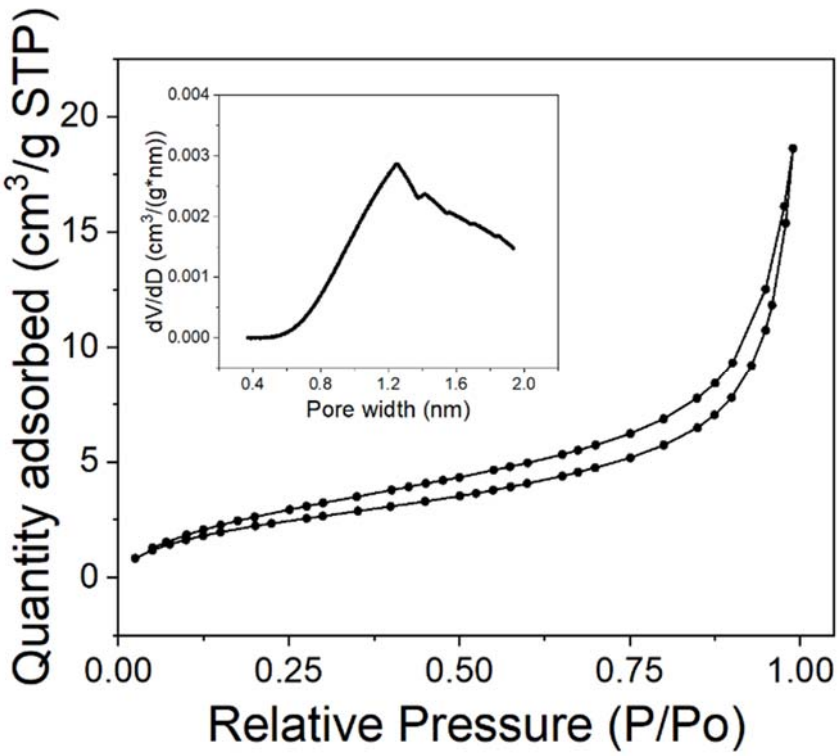

Supplementary Fig. 3 | BET isotherm plots for nitrogen adsorption capacity of 2 μm FEP. The insert is the pore distribution.

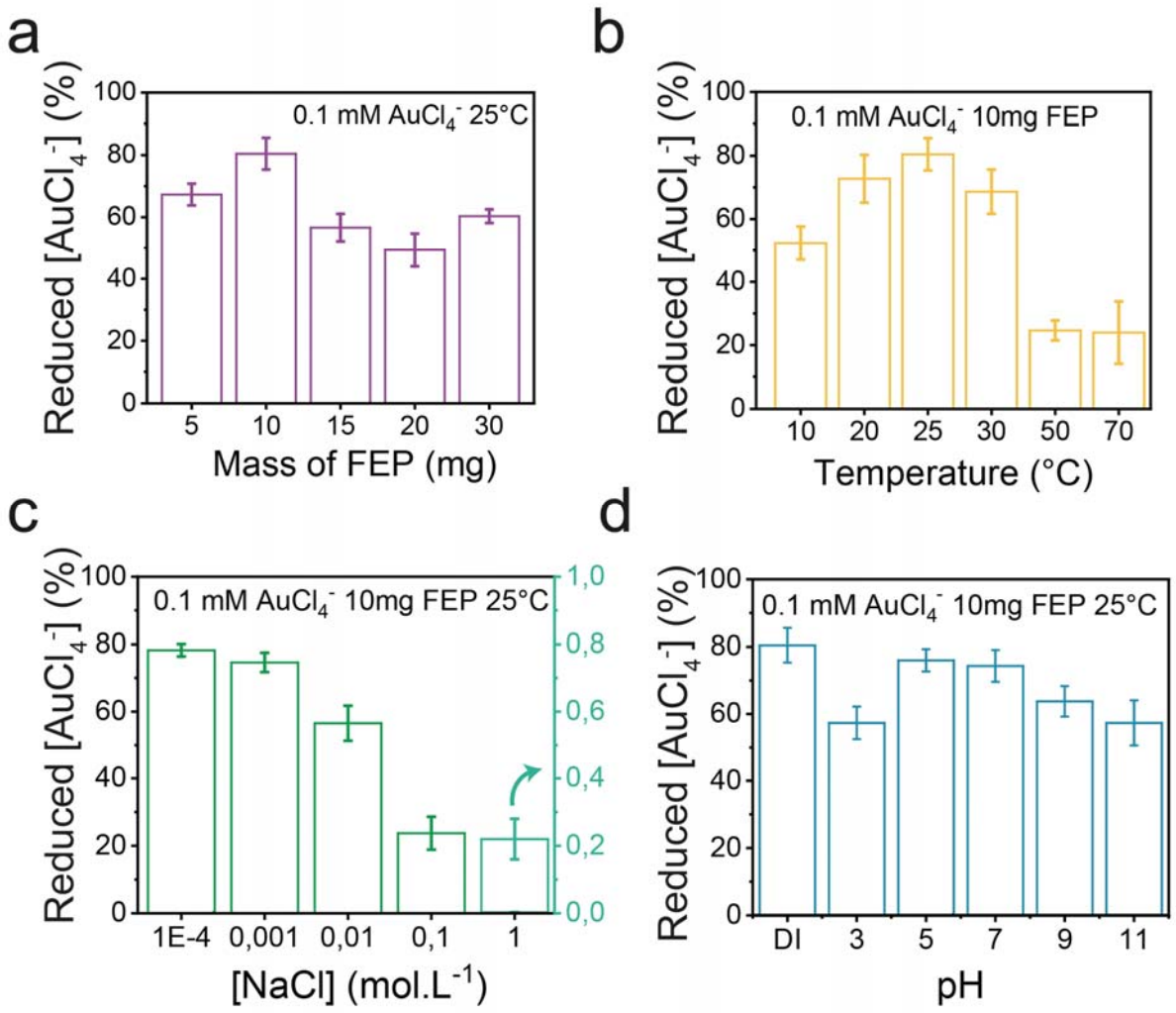

Supplementary Fig. 4 | Optimization of the reaction conditions. The influence of FEP (a) mass, (b) temperature, (b) NaCl concentration, and (d) pH on the reduction of the $AuCl_4^-$. For all figures, error bars represent standard deviations for 3 reproduced experiments.

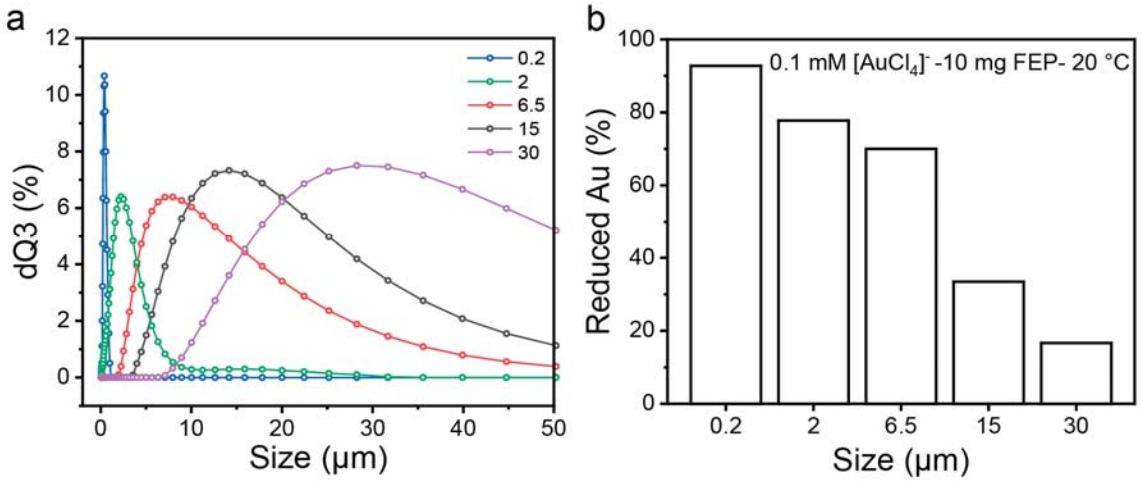

Supplementary Fig. 5 | Experiments with FEP powder of varying diameter. The size distribution (a) and gold extraction amount (b) of 0.2, 2, 6.5, 15, and 30 μm FEP powder.

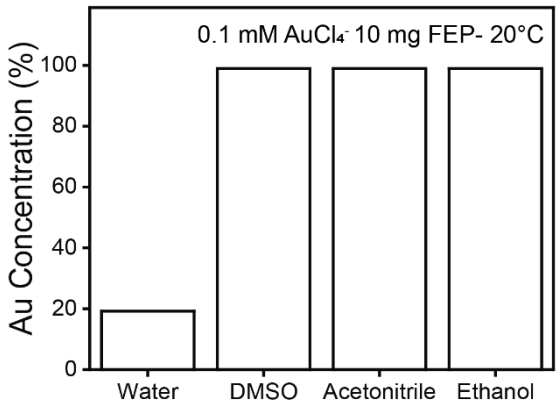

Supplementary Fig. 6 | $AuCl_4^-$ reduction by CEC in DMSO, acetonitrile, ethanol, and water.

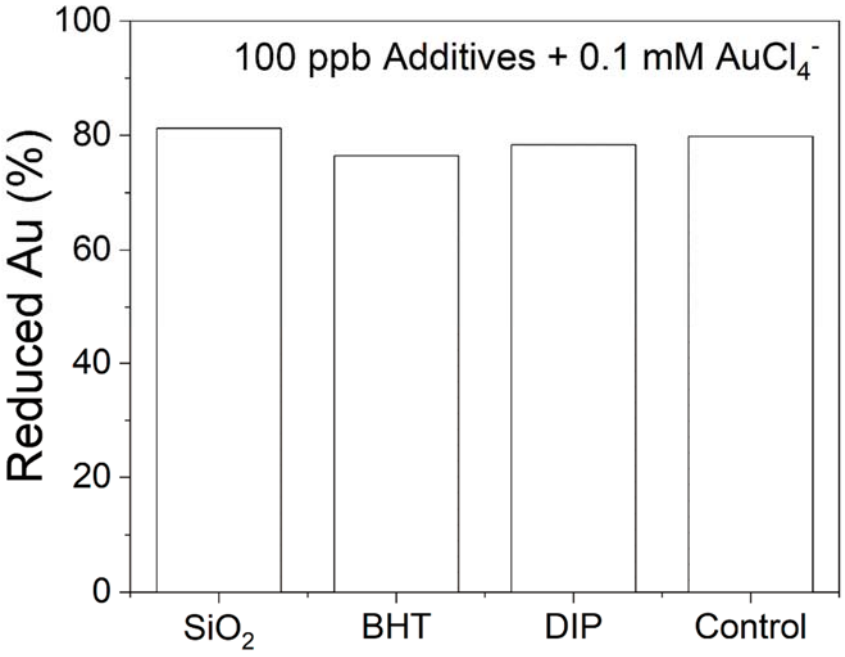

Supplementary Fig. 7 | Reduction of 0.1 mM $AuCl_4^-$ to which 100 ppb of various additives, including SiO_2, BHT (2,6-Di-tert-butyl-4-methylphenol), DIP (di(2-ethylhexyl)phthalate), in the presence of 10 mg FEP after one hour. The control is a standard experiment in absence of any additive in the solution.

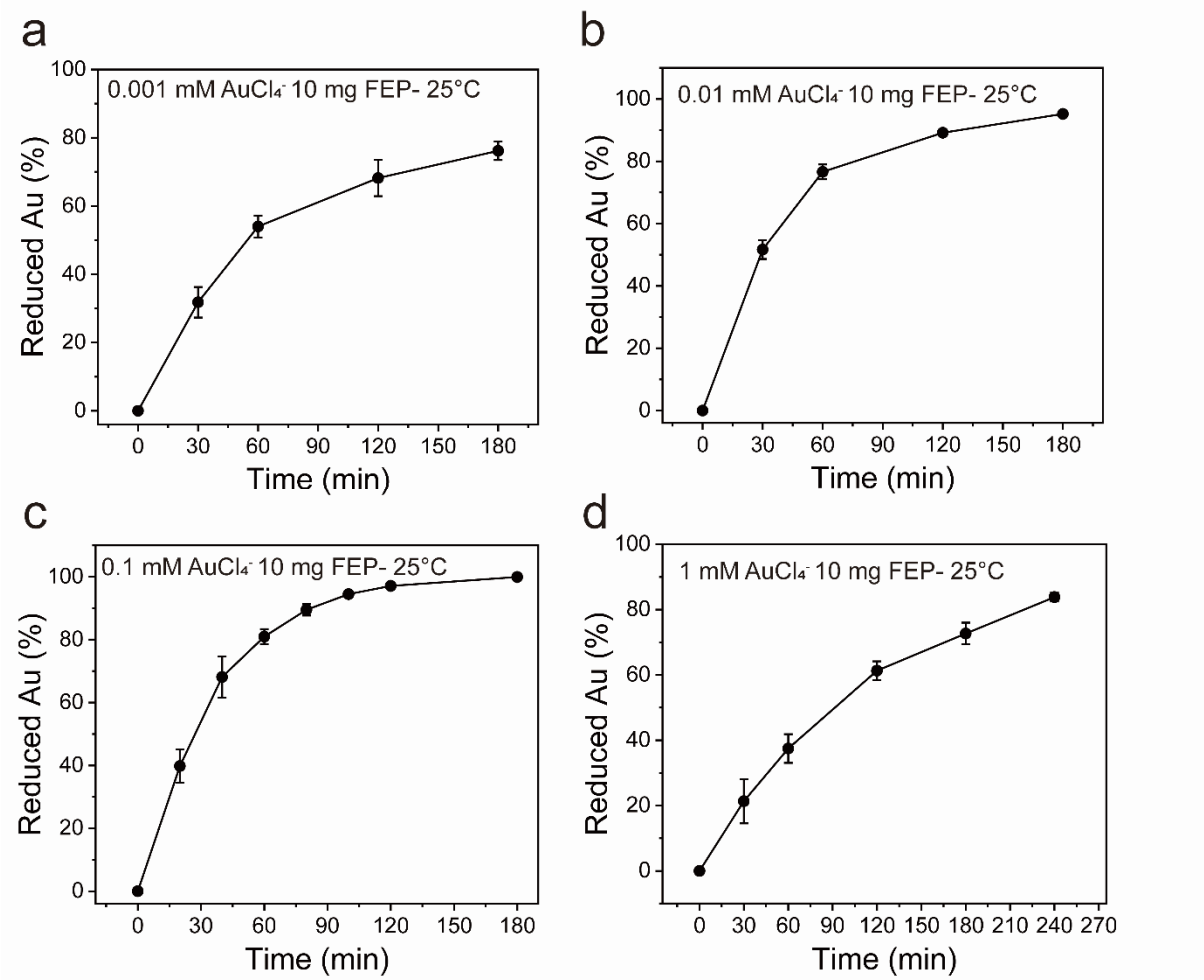

Supplementary Fig. 8 | Evolution of Au concentration in various concentrations including (a) 0.001 mM, (b) 0.01 mM, (c) 0.1 mM, and (d) 1 mM. Lines are guide to eyes. For all figures, error bars represent standard deviations for 3 reproduced experiments.

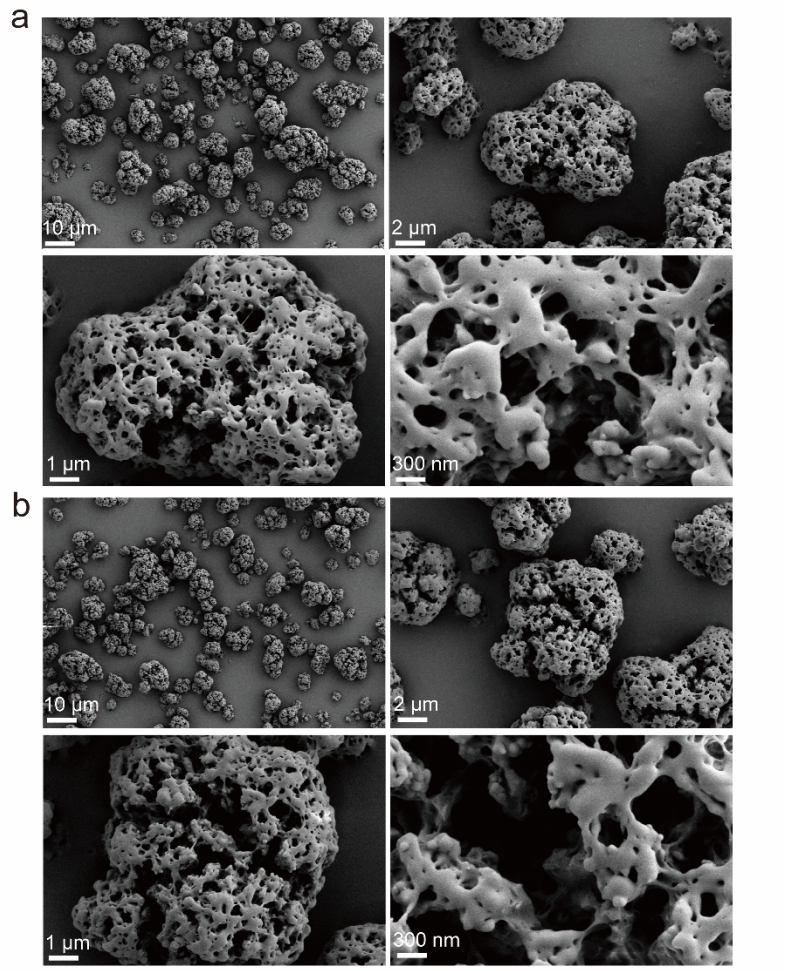

Supplementary Fig. 9 | Scanning electron microscopy of FEP (a) before and (b) after (b) reaction.

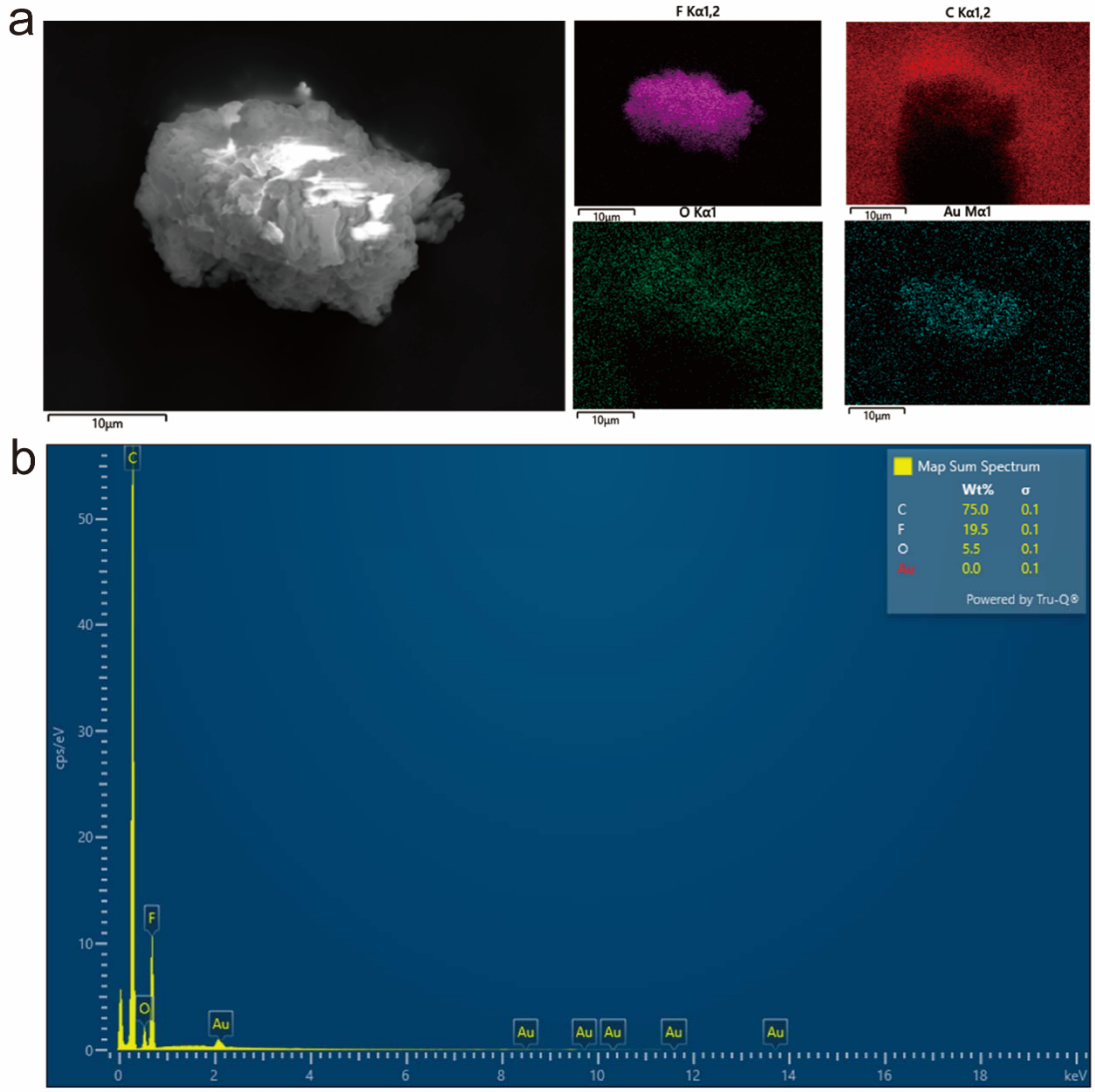

Supplementary Fig. 10 | (a) Energy dispersive spectrometer images and (b) spectrum of FEP after reaction.

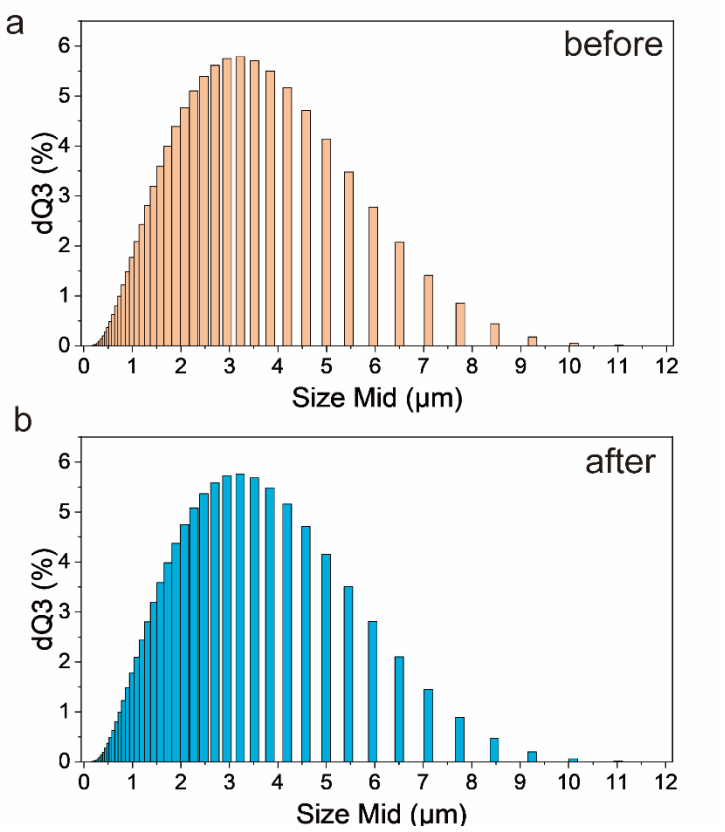

Supplementary Fig. 11 | Size distribution of FEP (a) before and (b) after the reaction.

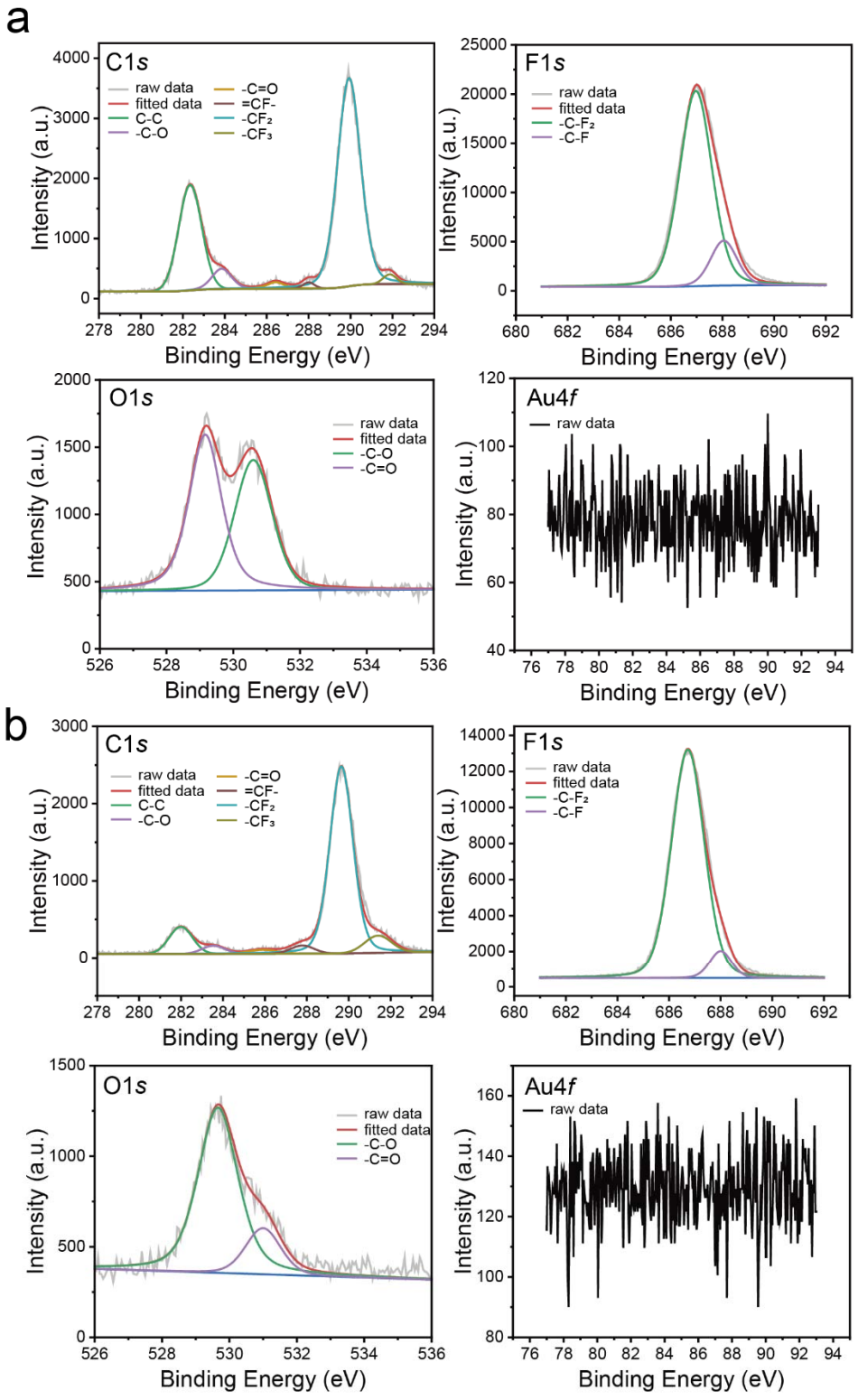

Supplementary Fig. 12 | X-ray photoelectron spectroscopy for FEP (a) before and (b) after reaction.

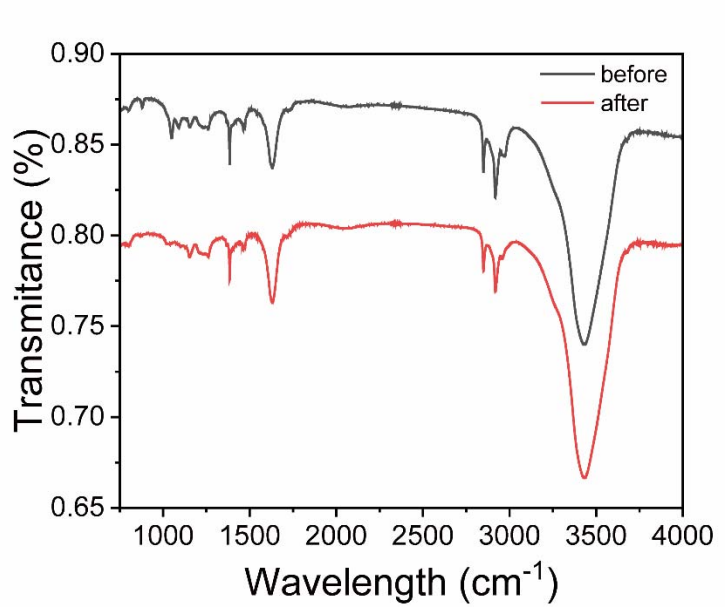

Supplementary Fig. 13 | Fourier Transform Infrared spectra of catalysis before and after the reaction.

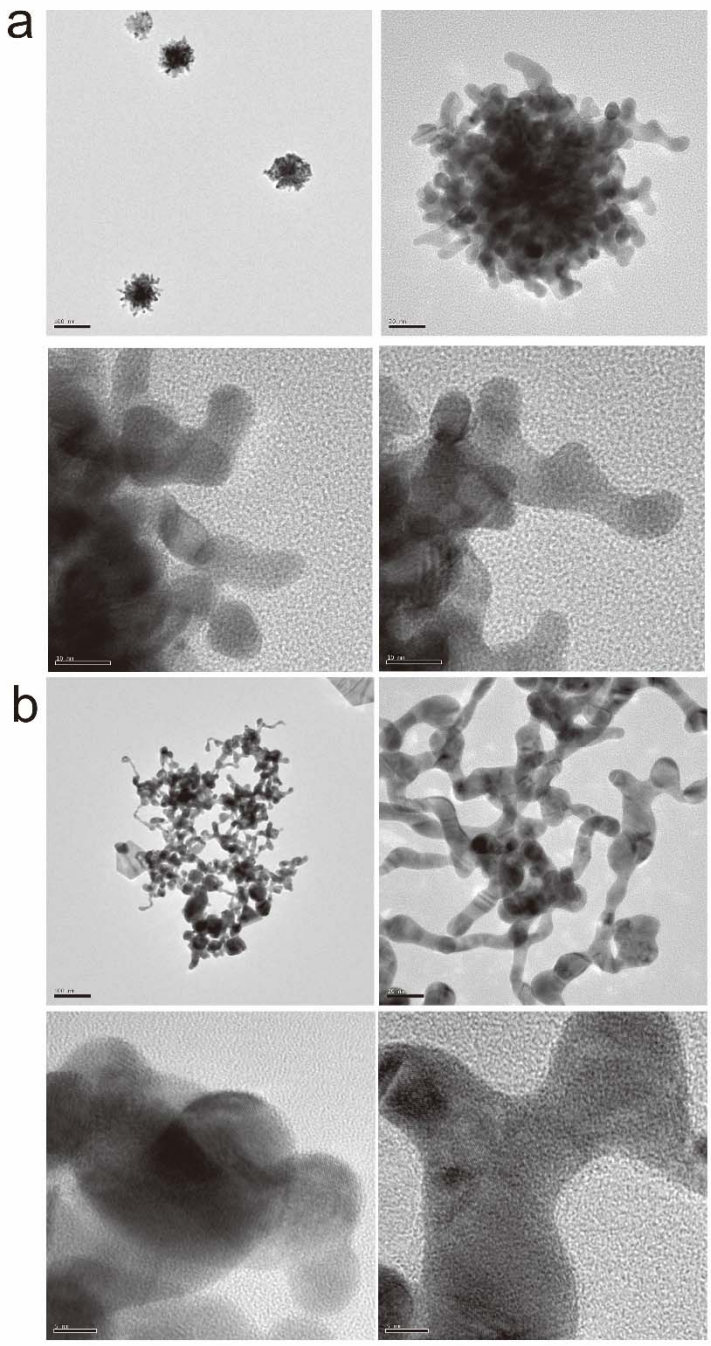

Supplementary Fig. 14 | Transmission electron microscopy images for Au dispersed in (a) water and (b) ethanol.

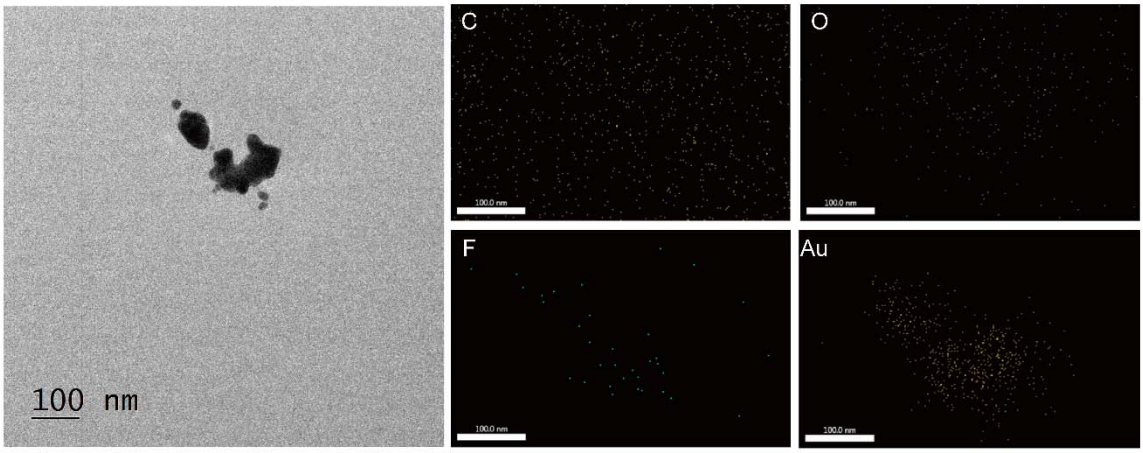

Supplementary Fig. 15 | Energy dispersive X-ray spectroscopy images of reduced Au.

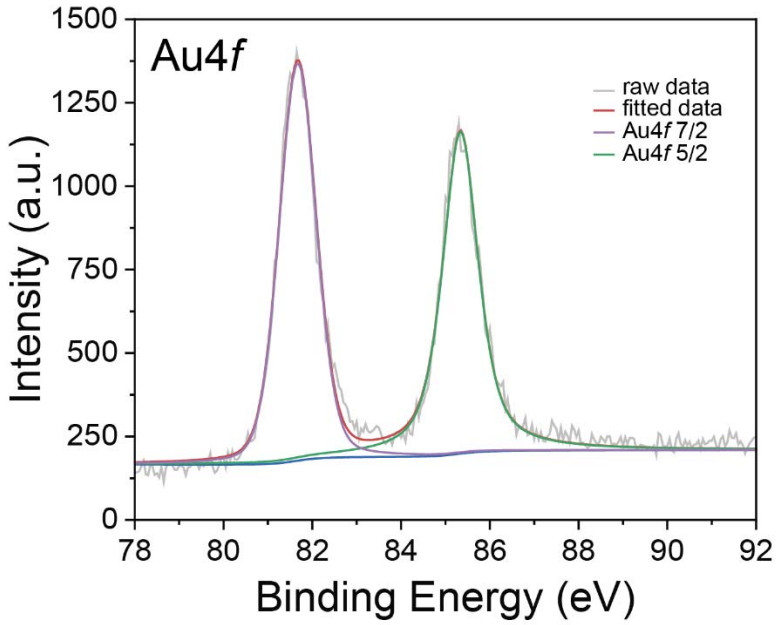

Supplementary Fig. 16 | XPS Au4*f* spectra of reduced gold.

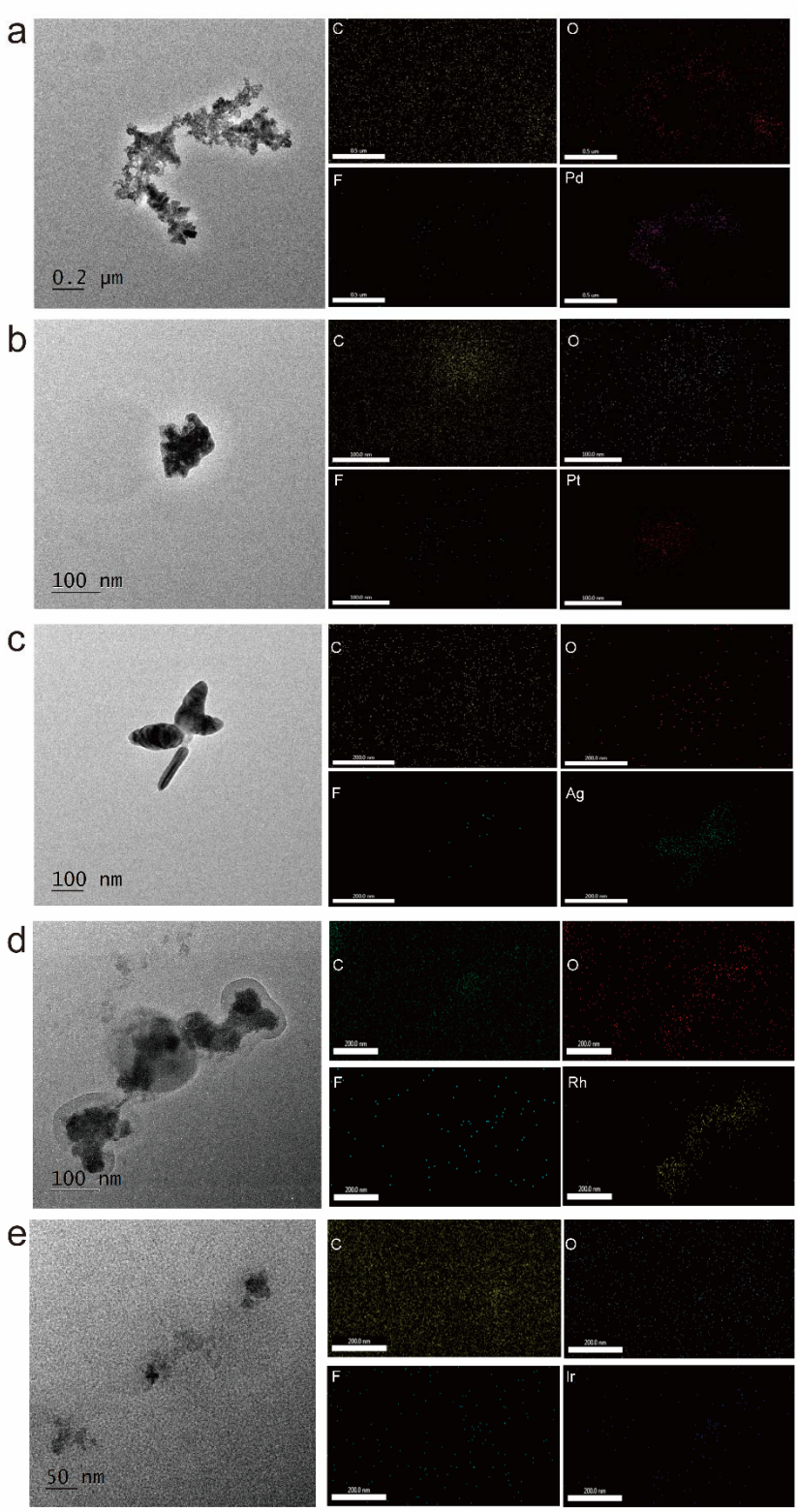

Supplementary Fig. 17 | Energy dispersive X-ray spectroscopy images of reduced (a) Pd, (b) Pt, (c) Ag , (d) Rh , and (e) Ir.

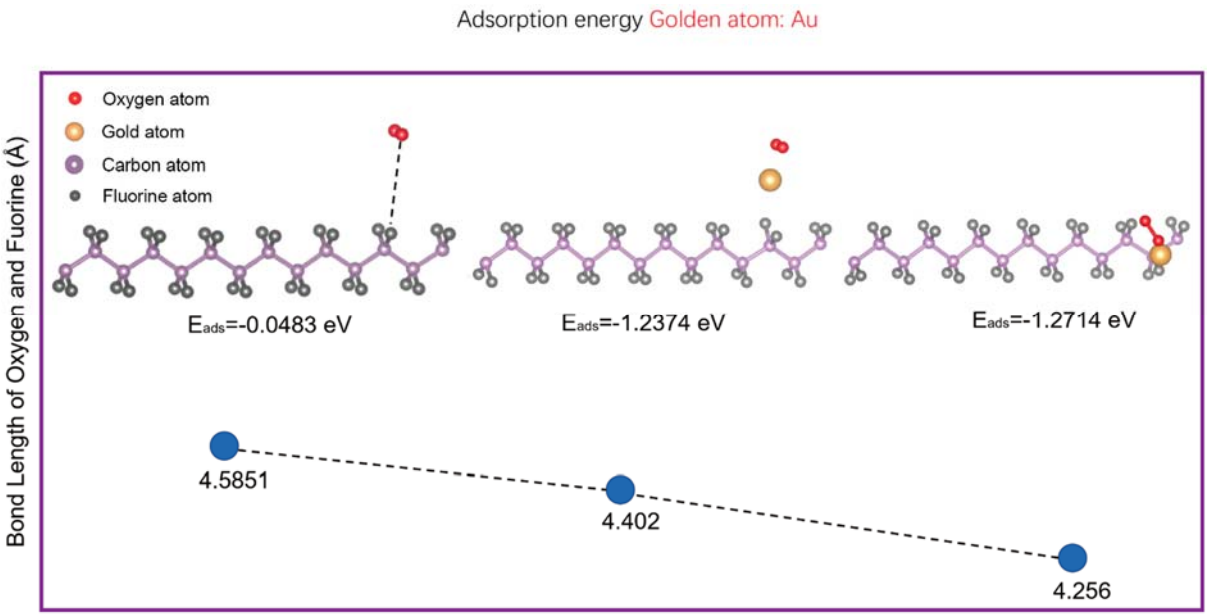

Supplementary Fig. 18 | Calculated distance between O of oxygen and F, and adsorption energy for PTFE and O_2. Carbon: Purple, Grey: Fluoride, Red: Oxygen, Yellow: Gold.

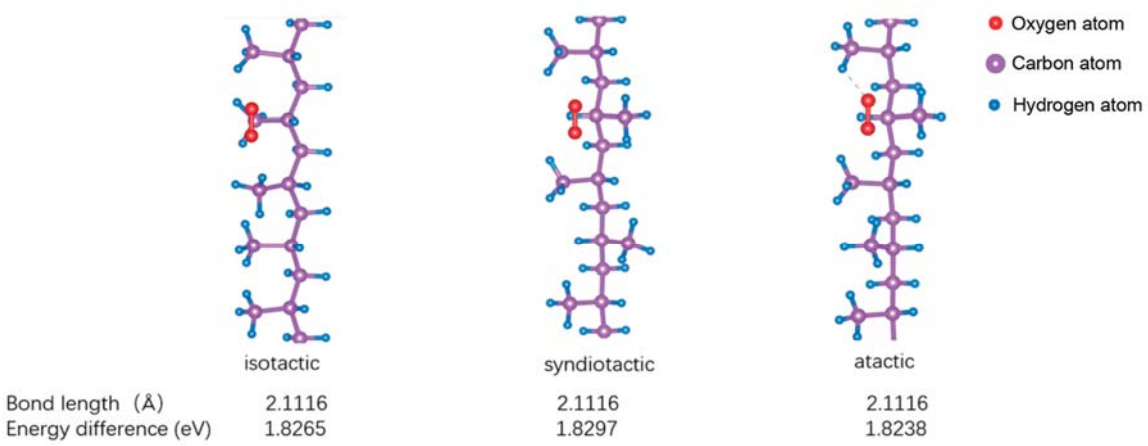

Supplementary Fig. 19 | Simulated energy difference $\Delta E(HOMO_{(PTFE)}- \pi_{(O2)})$ for isotactic, syndiotactic and atactic PP. Carbon: purple, Hydrogen: blue, Oxygen: red.

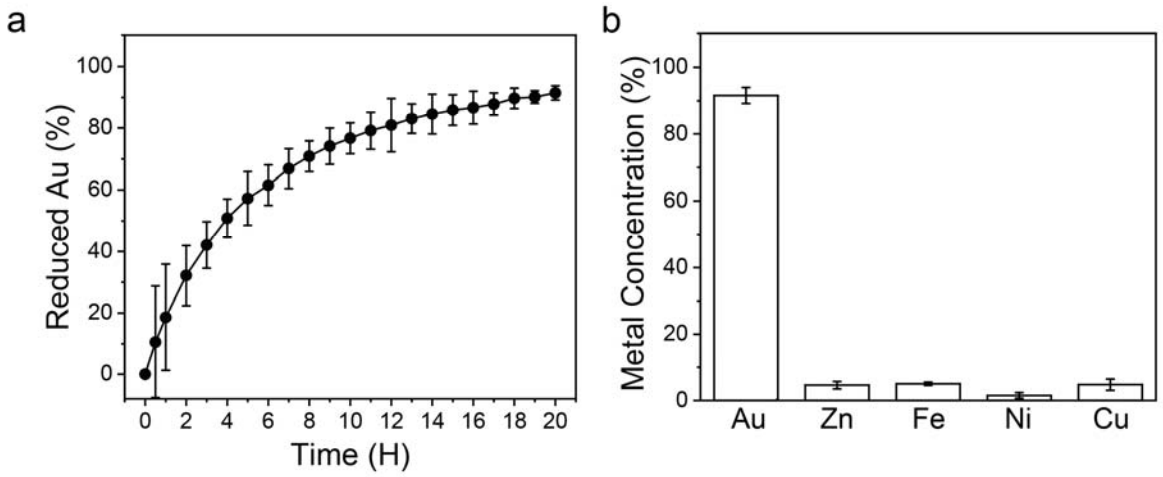

Supplementary Fig. 20 | Real world application for electroplating waste. (a) Evolution of Au concentration from electroplating waste. Lines are guide to eyes. (b) Amount of Au and other metals that were extracted from e-waste. For all figures, error bars represent standard deviations for 3 reproduced experiments.

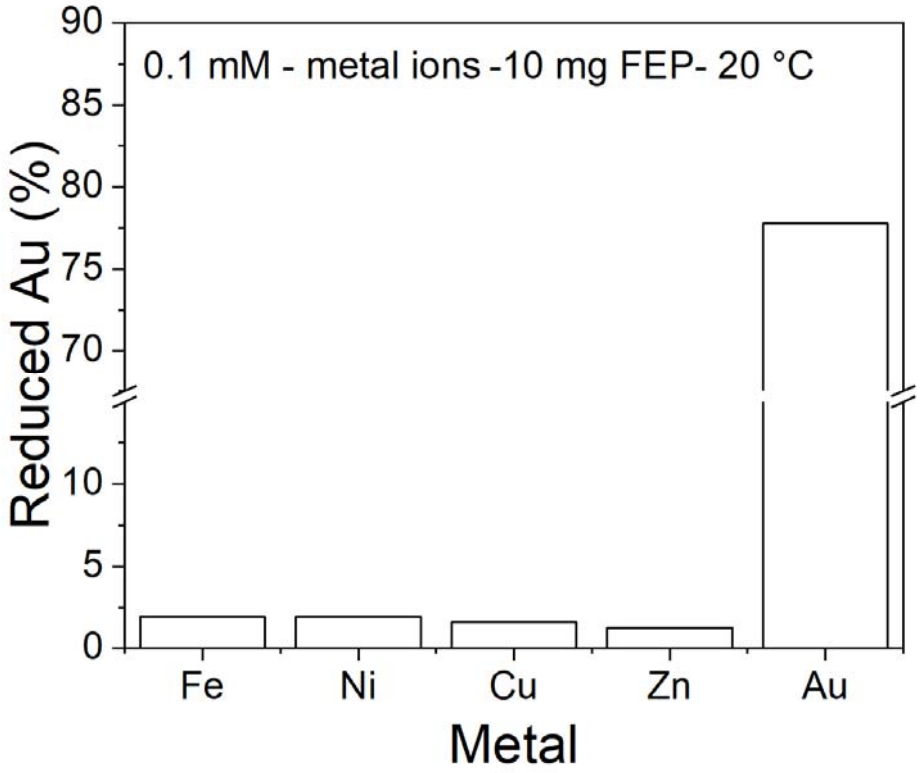

Supplementary Fig. 21 | Fe, Ni, Cu, Zn, and Au extraction amount in their anaerobic aqueous solution. The reaction condition is: 0.1 mM concentration for each ion with 10 mg FEP, in anaerobic conditions at 20 °C.

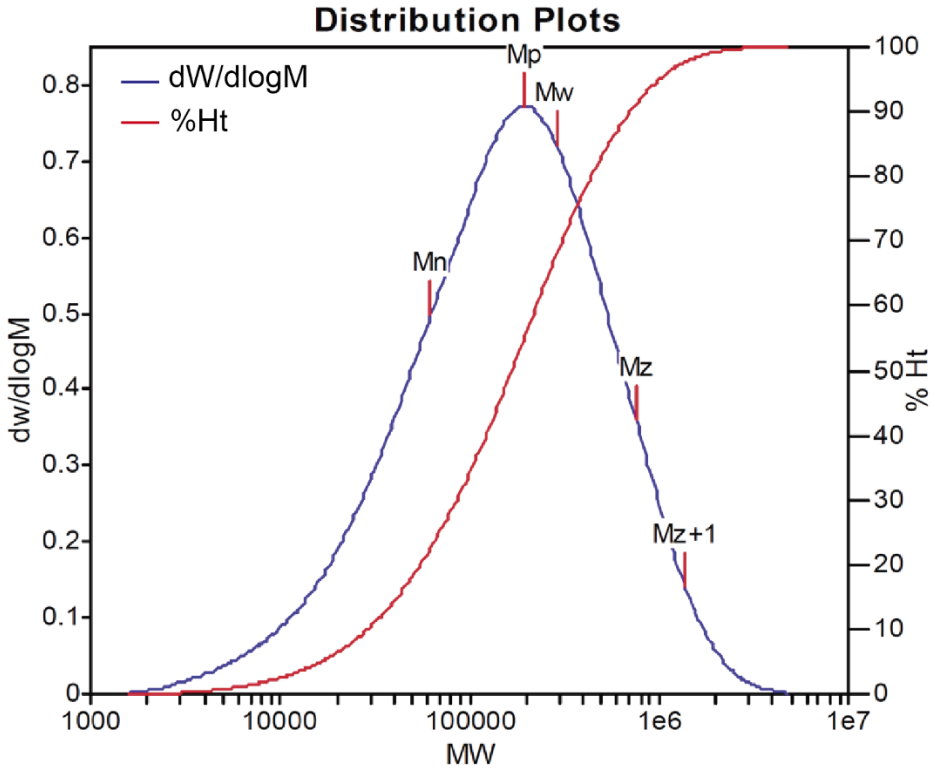

Supplementary Fig. 22 | GPC analysis of pristine PP. Mn=62672, Mw=289392, Mz=755130.

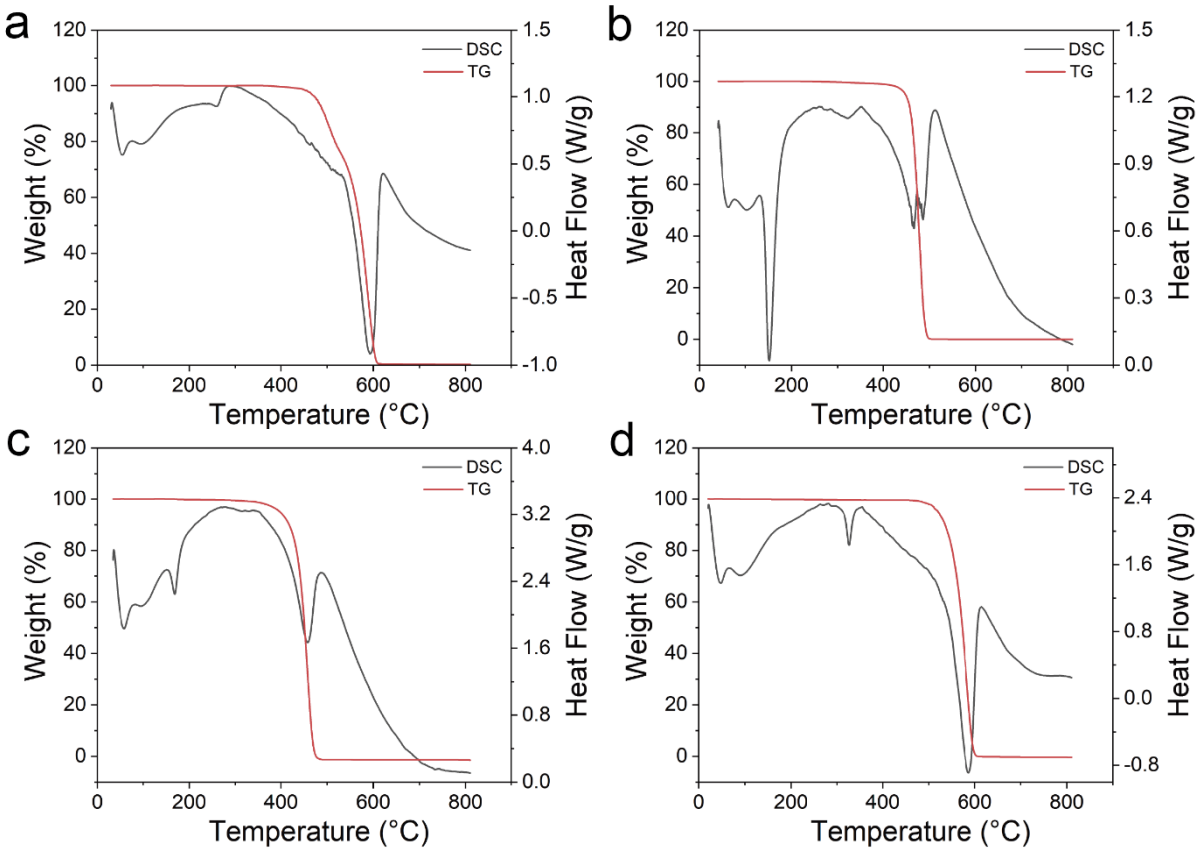

Supplementary Fig. 23 | TG-DSC analysis of pristine (a) FEP, (b) HDPE, (c) PP, and (d) PTFE.

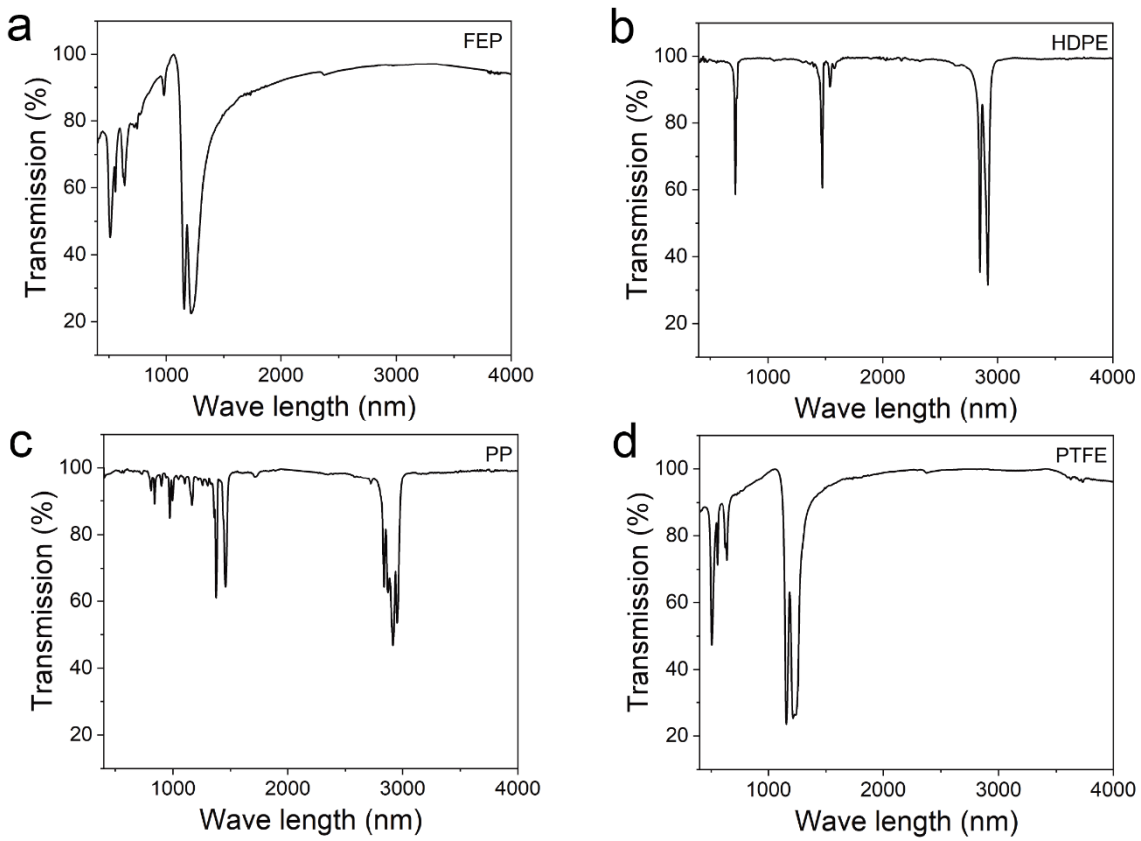

Supplementary Fig. 24 | Fourier Transformed Infra-Red Spectroscopy (FTIR) of pristine (a) FEP, (b) HDPE, (c) PP, and (d) PTFE.

Supplementary Fig. 25 | Photograph of reactor. The seal consists of a PTFE gasket, rubber ring and silica gel grommet.

Supplementary Table 1. Intermittent (Ultrasonication 30 min ON/30 min OFF, with a total ON time of 60 min) and continuous (60 min ON) result for 120 W 40 kHz and 60 W 40 kHz ultrasonication.

Time (min)	Gold extraction rate (%)	
	40 kHz, 120 W	40 kHz, 60 W
30	44.37197	19.68413
60	43.88840	19.13771
90	77.65794	32.96148
120	77.00936	32.39498
60 (continuous)	77.75359	33.03139

Supplementary Table 2. Surface properties of different sizes of FEP powder.

Size (um)	Specific surface area ($m^2 g^{-1}$)	Total pore volume ($cm^3 g^{-1}$)	Average pore diameter (nm)	Porosity (ρ=2.15 $cm^3 g^{-1}$)
0.2	88.458	0.24970	11.290	0.536877
2	9.023	0.02880	12.770	0.061920
6.5	5.159	0.02356	18.260	0.050654
15	4.017	0.01005	10.000	0.021608
30	3.997	0.00990	9.906	0.021285

Supplementary Table 3. Literature Review.

[Au] ppm	Types of Au Ion	Method	Material	Extraction Capacity ($mg\ g^{-1}$)	Extraction time (h)	Reference
10	$AuCl_4^-$	Adsorbent	Fe-BTC/PpPDA	96	0.033	9
20			COP-180	100	0.5	10
12.5			TDAC	17.5	24	11
100			TDAC	30	24	
14.8	$Au(S_2O_3)_2^{3-}$		MoS2/CS Aerogel	50	22	12
116			MoS2/CS Aerogel	600	22	
9.7			MoS2/CS Aerogel	20	22	
150			UiO-66-TA	260		13
80			CSGO5	400	16	14
100	$AuCl_4^-$		UiO-66	60	0.41666666	15
100			UiO-66-NH2	100	3	
150			UiO-66-TU	275		16
100			barley straw carbon	256	1	17
50			L-Lysine modified, crosslinked chitosan resin	13	4	18
40			cross-linked lignocatechol	40	24	19
60	Au^{3+}		modified wheat straw	125	24	20
100			CNT-MoS2	1000	4	21
20			PAF-1-thiourea	250	24	22
100	$Au(S_2O_3)_2^{3-}$		MoS2/ZnS	1120	5	23
50			MsS2/Zns	500	5	
100	$AuCl_4^-$		rGo nanosheets at 25C	1880	24	24
10				1850	24	
1				1180	24	
0.1				690	24	
0.197	$AuCl_4^-$	CEC	FEP	0.75609	3	This work
1.97			FEP	9.3872	3	
19.7			FEP	95	3	
197			FEP	722.5	3	

Supplementary Table 4. D-spacing and SAED analysis of reduced metals.

Au		d(111)		Rh		d(111)	d(111)
	HRTEM	2.35			HRTEM	2.2	2.19
	SAED	2.35			SAED	2.2	
	PDF#04-0784	2.355			PDF#04-0784	2.196	
Ir		d(111)	d(111)	Pt		d(111）	d(111)
	HRTEM	2.226	2.231		HRTEM	2.12	2.135
	SAED	2.22			SAED	2.27	
	PDF#06-0598	20.33			PDF#04-0802	2.26	
Pd		d(111)		Ag		d(111)	
	HRTEM	2.219			HRTEM	2.397	
	SAED	2.25			SAED	2.36	
	PDF#46-1043	2.246			PDF#04-0784	2.359	

Supplementary References

1. Lin, S., Chen, X. & Wang, Z. L. Contact Electrification at the Liquid–Solid Interface. *Chem. Rev.* **122**, 5209–5232 (2022).
2. Lin, S., Xu, C., Xu, L. & Wang, Z. L. The Overlapped Electron-Cloud Model for Electron Transfer in Contact Electrification. *Adv. Funct. Mater.* **30**, 1909724 (2020).
3. Berbille, A. *et al.* Mechanism for Generating H2O2 at Water-Solid Interface by Contact-Electrification. *Adv. Mater.* **n/a**, 2304387.
4. Zhao, Y. *et al.* The process of free radical generation in contact electrification at solid-liquid interface. *Nano Energy* **112**, 108464 (2023).
5. Song, W.-Z. *et al.* Insulator polymers achieve efficient catalysis under visible light due to contact electrification. *Water Res.* **226**, 119242 (2022).
6. Wang, Z. *et al.* Contact-electro-catalysis for the degradation of organic pollutants using pristine dielectric powders. *Nat. Commun.* **13**, 1–9 (2022).
7. Vogel, Y. B. *et al.* The corona of a surface bubble promotes electrochemical reactions. *Nat. Commun.* **11**, 6323 (2020).
8. Chen, B. *et al.* Water–solid contact electrification causes hydrogen peroxide production from hydroxyl radical recombination in sprayed microdroplets. *Proc. Natl. Acad. Sci.* **119**, e2209056119 (2022).
9. Sun, D. T., Gasilova, N., Yang, S., Oveisi, E. & Queen, W. L. Rapid, Selective Extraction of Trace Amounts of Gold from Complex Water Mixtures with a Metal–Organic Framework (MOF)/Polymer Composite. *J. Am. Chem. Soc.* **140**, 16697–16703 (2018).
10. Hong, Y. *et al.* Precious metal recovery from electronic waste by a porous porphyrin polymer. *Proc. Natl. Acad. Sci.* **117**, 16174–16180 (2020).

11. Dwivedi, A. D., Dubey, S. P., Hokkanen, S., Fallah, R. N. & Sillanpää, M. Recovery of gold from aqueous solutions by taurine modified cellulose: An adsorptive–reduction pathway. *Chem. Eng. J.* **255**, 97–106 (2014).

12. Chen, P., Liang, Y., Yang, B., Jia, F. & Song, S. In Situ Reduction of Au(I) for Efficient Recovery of Gold from Thiosulfate Solution by the 3D MoS2/Chitosan Aerogel. *ACS Sustain. Chem. Eng.* **8**, 3673–3680 (2020).

13. Wang, C. *et al.* Highly selective recovery of Au(III) from wastewater by thioctic acid modified Zr-MOF: Experiment and DFT calculation. *Chem. Eng. J.* **380**, 122511 (2020).

14. Liu, L. *et al.* Preparation and characterization of chitosan/graphene oxide composites for the adsorption of Au(III) and Pd(II). *Talanta* **93**, 350–357 (2012).

15. Lin, S. *et al.* Effective adsorption of Pd(II), Pt(IV) and Au(III) by Zr(IV)-based metal–organic frameworks from strongly acidic solutions. *J. Mater. Chem. A* **5**, 13557–13564 (2017).

16. Wu, C. *et al.* Specific Recovery and In Situ Reduction of Precious Metals from Waste To Create MOF Composites with Immobilized Nanoclusters. *Ind. Eng. Chem. Res.* **56**, 13975–13982 (2017).

17. Chand, R. *et al.* Selective adsorption of precious metals from hydrochloric acid solutions using porous carbon prepared from barley straw and rice husk. *Miner. Eng.* **22**, 1277–1282 (2009).

18. Fujiwara, K., Ramesh, A., Maki, T., Hasegawa, H. & Ueda, K. Adsorption of platinum (IV), palladium (II) and gold (III) from aqueous solutions onto l-lysine modified crosslinked chitosan resin. *J. Hazard. Mater.* **146**, 39–50 (2007).

19. Parajuli, D. *et al.* Selective Recovery of Gold by Novel Lignin-Based Adsorption Gels. *Ind. Eng. Chem. Res.* **45**, 8–14 (2006).

20. Wang, J., Li, J. & Wei, J. Adsorption characteristics of noble metal ions onto modified straw bearing amine and thiol groups. *J. Mater. Chem. A* **3**, 18163–18170 (2015).

21. Liu, F., You, S., Wang, Z. & Liu, Y. Redox-Active Nanohybrid Filter for Selective Recovery of Gold from Water. *ACS EST Eng.* **1**, 1342–1350 (2021).

22. Ma, T. *et al*. Efficient Gold Recovery from E-Waste via a Chelate-Containing Porous Aromatic Framework. *ACS Appl. Mater. Interfaces* **12**, 30474–30482 (2020).

23. Zhan, W., Yuan, Y., Yang, B., Jia, F. & Song, S. Construction of MoS2 nano-heterojunction via ZnS doping for enhancing in-situ photocatalytic reduction of gold thiosulfate complex. *Chem. Eng. J.* **394**, 124866 (2020).

24. Li, F. *et al*. Highly efficient and selective extraction of gold by reduced graphene oxide. *Nat. Commun.* **13**, 4472 (2022).